TiO_{2}-SnO_{2}:F interfacial electronic structure investigated by soft x-ray absorption spectroscopy

Coleman X. Kronawitter, Mukes Kapilashrami, Jonathan R. Bakke, Stacey F. Bent, Cheng-Hao Chuang, Way-Faung Pong, Jinghua Guo, Lionel Vayssieres, and Samuel S. Mao

Phys. Rev. B **85**, 125109 — Published 9 March 2012

DOI: 10.1103/PhysRevB.85.125109

TiO_2 – FTO interfacial electronic structure investigated by soft X-ray absorption spectroscopy

Coleman X. Kronawitter[a,b], Mukes Kapilashrami[c], Jonathan R. Bakke[d], Stacey F. Bent[d], Cheng-Hao Chuang[c,e], Way-Faung Pong[e], Jinghua Guo[c], Lionel Vayssieres[f *], Samuel S. Mao[a,b *]

[a]Department of Mechanical Engineering, University of California at Berkeley, Berkeley, CA 94720 (USA)
[b]Environmental Energy Technologies Division, Lawrence Berkeley National Laboratory, Berkeley, CA 94720 (USA)
[c]Advanced Light Source, Lawrence Berkeley National Laboratory, Berkeley, CA 94720 (USA)
[d]Department of Chemical Engineering, Stanford University, Stanford, CA 94305 (USA)
[e]Department of Physics, Tamkang University, Tamsui, Taiwan (ROC)
[f]International Research Center for Renewable Energy, State Key Laboratory of Multiphase Flow in Power Engineering, Xi'an Jiaotong University, Shaanxi 710049 (China)

*Corresponding Authors
ssmao@lbl.gov
lionelv@xjtu.edu.cn

The electronic structure of the titanium dioxide (TiO_2) - fluorine-doped tin dioxide (FTO) interface is investigated by soft X-ray absorption spectroscopy using synchrotron radiation. The measurements probe the site- and symmetry-selected unoccupied density-of-states, and reflect a complex interaction between an early transition metal oxide (d^0) semiconductor and a post-transition metal oxide (d^{10}) degenerate semiconductor. The distinct interfacial electronic structure of TiO_2-FTO is established by contrasting spectra with those for anatase and rutile TiO_2, FTO, and ZnO-FTO and CdO-FTO interfaces. Oxygen 1*s* absorption spectra, which relate to the O 2*p* partial density-of-states of the conduction band, indicate that the interface is associated with a reduction in Ti *d* - O *p* orbital hybridization and an alteration of the TiO_2 crystal field. These observations are consistent with measured titanium 2*p* absorption spectra, which in addition provide evidence for distortion of long-range order around the cation site in the interfacial TiO_2. The TiO_2-FTO interface is a functional component of a number of optoelectronic devices, perhaps most notably within the anode structure of solar cell architectures. In non-equilibrium conditions such as those found in operating solar cells interfacial electronic structure directly influences performance, for instance by modifying the quasi-Fermi level of electrons and the potential distribution at the transparent electrode.

Keywords: Electronic structure, oxide heterostructures, titanium dioxide, X-ray absorption spectroscopy

I. Introduction

Performance in modern optoelectronics is increasingly reliant on the efficiency of interfacial processes, which are directly influenced by the character and occupancy of electronic states near the interface. Devices designed to absorb or emit light contain layers of organic or inorganic heterostructures, which either function as active components or which facilitate the extraction or injection of electrons from or to the optically active phases. The interfacial regions of heterostructures, which can extend several nanometers beyond their actual atomic interfaces, can be characterized by abrupt or gradual changes in chemical, structural, and electronic properties.[1] The nature of these atomic- and molecular-level interactions is not restricted to academic interest; the macroscopic performance of modern technologies is often reliant on their presence. Here we can consider for example the various incarnations of the excitonic solar cell,[2] and its inorganic counterpart the quantum dot solar cell,[3] whose very operation requires exciton dissociation and electron transfer processes, which are interfacial phenomena. In general the significance of heterostructure properties is amplified in nanodevices, the large junction areas within which contribute considerably to the overall device functionality.

In transition metal oxide heterostructures, charge transfer, covalent bonding, and orbital reconstruction effects modify the *d* orbital character and occupancy at the interface.[4] These effects are expressed through a number of new discoveries whose related technologies will rely on precise knowledge of the interface electronic structure, such as those utilizing interfacial conductivity,[5] magnetism,[6] or electron enrichment.[7] Size effects in low-dimensional oxides further influence interfacial chemistry[8] and electronic structure through enhancements in orbital hybridization[9] and through quantum confinement.[10]

Here we study the electronic structure of the interface of titanium dioxide (TiO_2) and fluorine-doped tin dioxide (SnO_2:F, FTO), one of the most commonly utilized transparent conductive oxides (TCO). FTO is the preferred TCO for numerous optoelectronic applications and is notable for its thermal stability over a wide range of processing temperatures. The buried interfaces are studied by synchrotron-based soft X-ray absorption spectroscopy (XAS), which provides spectra related to the site- and symmetry-selected unoccupied density of states. The key experimental requirement is the deposition of ultrathin layers, whose feature dimensions should not exceed the inelastic mean free

path of electrons (*ca.* 1-10 nm). This enables the measurement of electron yields generated from transitions originating exclusively from the interfacial region upon synchrotron soft X-ray irradiation. For comparative purposes we examine some aspects of CdO- and ZnO-FTO interfaces (all post-transition metal oxides), mainly to highlight the relative chemical sensitivity and specificity of the TiO_2 phase. We adopt the notation SnO_2:F to refer to the FTO phase, and ZnO and CdO to refer to the binary post-transition metal oxides, which are expected to remain stoichiometric in these conditions due to the very high ionization potentials of monovalent cations. The TiO_2 phase is strongly influenced by the substrate as will be discussed in detail herein. However, for convenience we refer to the ultrathin titanium oxide as TiO_2, given that similar preparation conditions for thicker films produce stoichiometric TiO_2.[11]

Comprehensive understanding of the electronic structure of oxide-TCO interfaces contributes to continuing efforts to optimize a number of optoelectronic devices of considerable social consequence. The oxide-TCO interface be found in dye-sensitized,[12,13,14] quantum dot-sensitized,[15] organic,[16] and solid-state solar cells,[17,18,19], in light emitting[20] and organic light emitting diodes, as well as in solar water splitting photoanodes.[21] In nanodevices the interface may result from the direct growth of nanomaterials onto TCO electrodes[22] or through the use of seed layers[23] to facilitate nanomaterial growth. In all cases, during device operation electrons are transported through the interfacial region, where they interact with the interface electronic structure. For instance, in dye-sensitized solar cells the open circuit potential can be limited by recombination at the metal oxide-TCO interface.[24] Additionally it has recently been demonstrated that annealing α-Fe_2O_3 photoanodes at high temperatures alters the nature of the α-Fe_2O_3-TCO interface, leading to a dramatic increase in water oxidation photocurrents in photoelectrochemical cells.[25] Another recent report, which has motivations similar to those in this study, has characterized the TiO_2-indium tin oxide interface electronic structure through photoemission spectroscopy.[26] A fundamental understanding of the oxide-TCO interface provides direction to address operational deficiencies at their physical source. To best facilitate these important fields, we fabricated heterostructures using techniques that realistically represent actual fabrication steps for these devices: use of commercial polycrystalline FTO substrates, low temperatures, and moderate pressures.

II. Experiment

Ultrathin films of TiO_2, ZnO, and CdO were fabricated by atomic layer deposition (ALD). Films were deposited onto commercial FTO substrates (Pilkington, TEC 7) at 150 °C utilizing titanium tetrachloride, diethyl zinc dimethyl cadmium, and water as the precursors. The pulsing sequence for each system was 3 s metal molecule, 60 s N_2 purge, 3 s water, and 60 s N_2 purge where the N_2 purge and carrier flow rate is constant at 80 SCCM. Six cycles of ZnO and CdO and 15 cycles of TiO_2 were performed so that the thickness of each oxide is 12 ± 2 Å [11,27]. Prior to measurement, all samples were annealed in air at 450 °C for 2 hrs (0.36 °C s^{-1} ramp rate from 23 °C to 450 °C), to ensure the crystallinity of all phases.

Soft X-ray absorption spectra were measured on Beamline 8.0 at the Advanced Light Source (ALS) at Lawrence Berkeley National Laboratory. Spectra were recorded in total electron yield mode (TEY), and were obtained by measurement of the sample drain photocurrent under irradiation with monochromatic light. The resolutions of the measurements were 0.4 eV at the O *K*-edge, 0.35 eV at the Sn *M*-edge, and 0.3 eV at the Ti *L*-edge. The incident radiation flux was monitored by the photocurrent produced in a gold mesh in the beam path. The photon energy was calibrated using the first peak of the anatase TiO_2 O l*s* absorption spectrum located at 530.8 eV. Absorption spectra for anatase and rutile TiO_2 were measured on Beamline 7.0.1.

III. Results and Discussion

Soft X-ray absorption spectroscopy probes the site- and symmetry-selected unoccupied density-of-states through an electronic transition between a localized core state and a valence state in the oxide materials. The large energy separation among core levels gives the technique elemental selectivity, the participation of valence electrons yields chemical state sensitivity, and the dipole nature of the transitions provides symmetry information. The probe is localized to one specific atomic site, around which the electronic structure is reflected as a partial density-of-states contribution.

To provide context to an analysis of interfacial X-ray absorption spectra, a few important distinctions are necessary to be made between TiO_2 and the post-transition metal oxides SnO_2, ZnO, and CdO. In bulk TiO_2, Ti ions have a $Ti^{4+}(3d^0)$ electronic configuration and the empty conduction band is comprised of Ti 3*d*, 4*s*, and 4*p* orbitals, with 3*d* orbitals dominant in the bottom of the conduction band. In contrast, in SnO_2 for example, Sn ions have a $Sn^{4+}(4d^{10}5s^05p^0)$ configuration, with 5*s* and 5*p* orbitals dominant in the conduction band minimum.[28] In addition, with a few exceptions the post-transition metal oxide cations have one preferred oxidation state, whereas in the transition metal oxides there is often a small energy difference between the d^n and d^{n+1} configurations. As a result, the transition metals typically have many stable oxides and their surface and interface chemistry is much more complex.[29] These complexities are evident in X-ray absorption spectra; their interpretation requires the inclusion of titanium oxide reference spectra. There are additional properties specific to the reference oxides examined which must be briefly addressed. The anisotropy[30] and surface polarity[31] of ZnO are important aspects of this material which directly influence electronic structure measurements. Additionally, the large electron accumulation in CdO,[32] associated with massive band bending, is not characteristic of TiO_2 and should be noted. These factors should not influence our

interpretations to any significant degree.

Oxygen ls soft X-ray absorption

Upon irradiation of the oxides with X-rays of sufficient energies, core O l*s* electrons are promoted to an excited state, which is coupled to the original state by the dipole selection rule.[33] The change in angular momentum quantum number (ΔL) must be ±1 – only the oxygen *p* character is probed. The existence of these transitions in itself is an indication of the partially covalent bonding in these materials.[34] For this application, O 1*s* spectra provide a useful representation of the unoccupied electronic structure at interfacial metal sites, because in these materials above the Fermi level empty bands are predominantly metal weight hybridized with O 2*p* character.

The O 1*s* absorption spectra for the bare SnO_2:F surface and the TiO_2-SnO_2:F, ZnO-SnO_2:F, and CdO-SnO_2:F interfaces are provided in Figure 1. The qualitatively similar spectrum measured for all cases confirms the validity of the ultrathin film approach to probe the interface: the buried SnO_2:F dominates the expression of O *p* states in each XAS measurement. In other words, because the inelastic mean free path is restricted to *ca.* 1-10 nm, the signal represents the O *p* states of the interface, defined as a region approximately 2 nm on either side of the atomic interface.

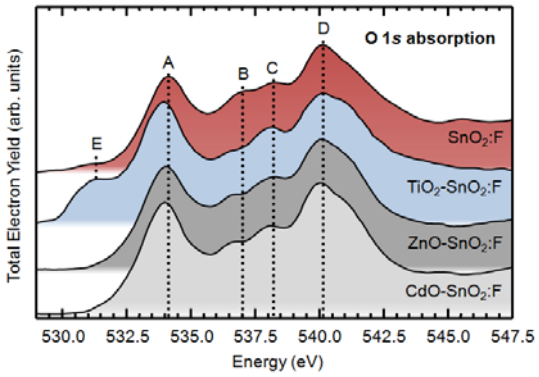

Figure 1. (Color online) O *K*-edge X-ray absorption spectra for (from top to bottom) SnO_2:F and the TiO_2-SnO_2:F, ZnO-SnO_2:F, and CdO-SnO_2:F interfaces.

The bottom of the conduction band of SnO_2 is comprised of Sn 5*s* orbitals, which hybridize with O 2*p* orbitals and are expressed in the O 1*s* absorption spectra as peak *A* in Figure 1. Peaks *B*, *C*, and *D* primarily correspond to the O 2*p* orbitals hybridized with Sn 5*p* orbitals deeper in the conduction band.[35] In the molecular orbital framework, peak *A* corresponds to transition to the a_g state, and peaks *B*, *C*, and *D* correspond to the successive transitions to the b_{1u}, b_{2u}, and b_{3u} states.[36] The a_g state reflects the partial density of states of the O_2 set of oxygen orbitals, which are perpendicular to the plane of the Sn_3O trigonal configuration, while the b_{1u}, b_{2u}, and b_{3u} states reflect a combination of the in-plane O_1 set and out-of-plane O_2 set.[35,37] Peak *E*, located in the pre-edge region at 531.4 eV, is found uniquely in TiO_2-SnO_2:F, and results from the hybridization of unoccupied Ti $d(t_{2g})$ levels with O 2*p* levels, which exist in the conduction bands of titanium oxides, as will be discussed in detail later in this report. Close inspection of the rising edge of peak *A* reveals additional intensity near 533.4 eV for all thin film samples. This is attributed to Ti 3*d*-, Zn 4*s*-, and Cd 5*s* - O 2*p* hybridized states, which exist in the respective conduction bands of the oxides.

Tin 3*d* soft X-ray absorption

The Sn $M_{4,5}$-edge X-ray absorption spectra, presented in Figure 2, describe transitions from Sn 3*d* levels to *p* or *f* states in the conduction band of SnO_2:F. The lower signal-to-noise ratio in comparison to those for O *K*-edge spectra results from the much lower X-ray absorption cross section of the *M*-edge. The conduction band minimum of SnO_2 is dominantly comprised of Sn 5*s* levels. Deeper in the conduction band the density-of-states is dominantly Sn *p* character.[38]

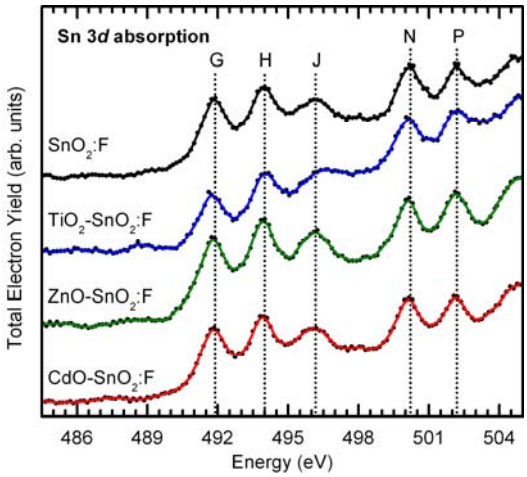

Figure 2. (Color online) Sn $M_{4,5}$-edge absorption spectra for bare SnO_2:F (black solid line), and the TiO_2-SnO_2:F (blue solid line), ZnO-SnO_2:F (green solid line), and CdO-SnO_2:F (red solid line) interfaces.

It is apparent in Figure 2 that Sn 3*d* absorption at the surface of SnO_2:F is largely unchanged by the formation of an interface with CdO and ZnO. Here we can consider the relative chemical stability of the post-transition metal oxides. High energies are required to add or remove electrons when these cations are coordinated with O^{2-} ligands, limiting the number of states accessible for the formation of defects, which have different electron configurations.[29] These spectra contrast with that of TiO_2-SnO_2:F, which contains a large distortion of the M_4 and M_5 bands. The broadening and overall reduction in resolution of these peaks compared to those for bare SnO_2:F has been found in X-ray absorption spectra for SnO.[39] Through consideration of high-surface-area SnO_2 aerogels, Kucheyev *et al.*[39] assigned the distortion to the presence of under-coordinated surface atoms. Ahn *et al.*[40] observed a similar broadening in their study of size-controlled SnO_2 nanoparticles, where increased broadening was found to be correlated with decreasing nanoparticle size. Broadening in this case was attributed to decreasing long-range order in SnO_2 crystals.

The small leading edge feature at 488.5 eV present in the M_5 band for TiO_2-SnO_2:F has been identified previously in SnO_2 aerogels[39] and nanoribbons.[41] It is suggested to be related to Sn *p* states that are created by oxygen vacancies and surface reconstruction. The spin orbit splitting creates an M_4 band counterpart that overlaps with peak *J*, which explains the dramatic distortion of this peak in our experiments. Surface reconstruction of this type will alter the Fermi level position of the heterostructure.[39] The presence of additional Sn *p* states, which have been assigned to exist both below[42] and above[39] the conduction band minimum, potentially alters the electronic structure of the conduction band. In order to confirm the presence of SnO_2 surface reconstruction, which is only observed indirectly here, more detailed analyses are required, for example those involving high-resolution transmission electron microscopy.

Titanium 3*d* band projected onto O 2*p* orbitals

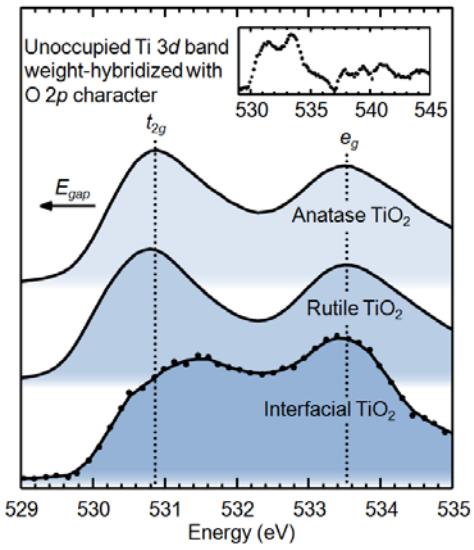

Figure 3. (Color online) Oxygen 1*s* absorption spectra for anatase TiO_2, rutile TiO_2, and TiO_2 thin film deposited on SnO_2:F. The interfacial TiO_2 spectrum was obtained by subtraction of the SnO_2:F O 1*s* absorption spectrum such that the intensity remained positive. The dashed

vertical lines indicate the positions of the Ti t_{2g} and e_g bands of anatase TiO_2. Inset provides the interfacial TiO_2 spectrum at higher energies.

The strong intensity of peak *E* in Figure 1, which corresponds primarily to unoccupied O 2*p* states, weight-hybridized in states with Ti 3*d* character,[9] enables more detailed analysis of the conduction band minimum of TiO_2 at its interface with SnO_2:F. The difference spectrum obtained by subtraction of the SnO_2:F O l*s* absorption spectrum from that of TiO_2-SnO_2:F (such that the resulting spectrum intensity is positive) is presented in Figure 3, with O l*s* absorption spectra of anatase and rutile TiO_2 included for comparison. The Ti 3*d* band of the O l*s* absorption spectrum (located from 529 eV to 535 eV[7]) is of primary interest to this study, and the difference spectrum in this energy range possesses a high signal-to-noise ratio, highlighting the importance of XAS for studying d^0 materials. The 4*sp* band is located at higher energies (inset of Figure 3) and possesses a larger energy spread, which is related to the degree of covalency in the material.[33] Increased broadening of this band is consistent with previous investigations of size effects in TiO_2,[9] as described in detail below. It is possible that the O 1*s* absorption spectrum of the underlying SnO_2:F, modified by the presence of the TiO_2, is not the same as that of bare SnO_2:F. (see discussion above on the Sn *M*-edge). The analysis of the difference spectrum that follows is conducted in the context of this unavoidable limitation.

In the oxides of titanium, Ti cations are surrounded by a distorted octahedron of oxygen anions, and the associated electrostatic fields split the *d* orbitals into a triply degenerate t_{2g} band (d_{xy}, d_{xz}, and d_{yz} orbitals) and a doubly degenerate e_g band (d_{x2-y2} and d_{z2} orbitals). The dashed vertical lines in Figure 3 show the positions of the t_{2g} and e_g bands hybridized with O 2*p* orbitals in the conduction band of anatase TiO_2. The center energies of the peaks corresponding to the e_g bands nearly overlap among anatase TiO_2, rutile TiO_2, and TiO_2-SnO_2:F. In contrast, the centroid of the t_{2g} peak for TiO_2-SnO_2:F lies at greater energies than reference titanium oxides.

The energy separation between the O 2*p* weights of the t_{2g} and e_g sub-bands is a reflection of the ligand-field strength, or the ligand-field splitting parameter Δ.[33] This parameter depends on the specific metal and ligand involved, as well as the oxidation state of the metal, and in general for a given metal the ligand field strength increases with increasing oxidation state. In the TiO_2-SnO_2:F interface, structural distortions in the lattice could change the symmetry of the cation site environment, which would be associated with a change in the ligand field. Interestingly, Soriano *et al.*[43] showed that structural disorder in TiO_2 induced by surface sputtering is associated with a 0.6 eV reduction in the ligand-field splitting, which was attributed to weaker Ti 3*d* - O 2*p* hybridization.

An alteration of the titanium oxide ligand-field is notable in this analysis of the interface electronic structure: the field influences the orientation of *d* orbitals around the metal ion in transition metal oxide systems, and by extension many of the system's physical properties. A large deviation of the ligand-field at the TiO_2-SnO_2:F interface from that of reference TiO_2 will influence electron conduction, which primarily takes place in empty Ti 3*d* orbitals. Significant alterations of the ligand-field strength suggest the presence of further distortion of the octahedral coordination of Ti.

The line shape of O l*s* absorption spectra in this energy range is additionally modified by size effects related to the high density of interface and surface states in nanoscale systems. Recently the size effect on the orbital character of TiO_2 nanoparticles over three orders of magnitude in average diameter (2-200 nm) has been reported[9]. It was determined that, as a consequence of the contracted nature of *d* orbitals, the hybridization of O 2*p* with Ti 4*s* orbitals is of greater importance in systems with nanoscale dimensionality and high concentrations of surface states. It is reasonable to assume in the present case that interface and surface states manifest as line broadening in the measured O l*s* absorption spectra, consistent with a relative enhancement of *s*-*p* orbital hybridization.

Titanium 2*p* soft X-ray absorption

Titanium *L*-edge absorption spectra were recorded to provide additional information on the interfacial cation site environment of TiO_2-SnO_2:F. For comparison, as above, spectra were recorded for anatase and rutile TiO_2 reference crystals. These spectra, presented in Figure 4a, possess four primary peaks, which result from the core-hole spin-orbit splitting of 2*p* levels and the crystal-field splitting of *d* orbitals discussed above.[44,45,46,47] Specifically, the L_3 band, located from 456 to 462 eV, represents the $2p_{3/2} \rightarrow 3d4s$ transition; the L_2 band located from 462 to 468 eV represents the $2p_{1/2} \rightarrow 3d4s$ transition. Peaks *T* and *W* reflect transitions to empty t_{2g} levels and Peaks *U, V*, and *Y* reflect transitions to empty e_g levels.

In the final state of the Ti 2*p* X-ray absorption process, the significant overlap of core and valence wavefunctions is expressed as multiplet effects, which remain largely unscreened in the solid state. These describe primarily atomic effects associated with electronic transitions (intra-ionic transitions) of the general form $2p^6d^n \rightarrow 2p^5d^{n+1}$. For this reason they can be simulated by calculations in the context of atomic multiplet theory with modifications to account for the crystal field and charge transfer effects,[48] or through multichannel multiple-scattering calculations.[49] The leading edge multiplet structure of TiO_2 (peaks *R* and *S*), have been assigned in analyses to $2p^6d^0 \rightarrow 2p^5d^1$ for Ti^{4+} in O_h symmetry.[50] The Ti 2*p* absorption spectra in Figure 4a indicate the Ti oxidation state in interfacial TiO_2 is primarily 4+.

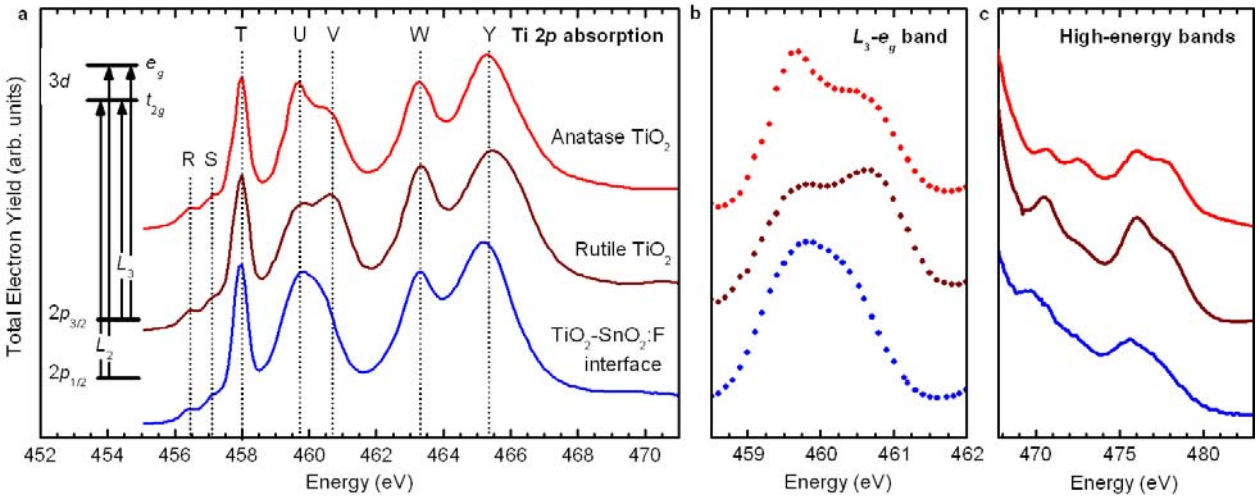

Figure 4. (Color online) Ti $L_{2,3}$-edge X-ray absorption spectra for (top to bottom) anatase TiO_2 (red), rutile TiO_2 (dark red), and TiO_2-SnO_2:F (blue). (a) Complete spectra; (b) L_3-e_g band; (c) High-energy bands, normalized to peak *Y*. (b) and (c) follow the same order and color convention as in (a).

We now consider the L_3-e_g band (peaks *U* and *V*, Figure 4b), which shows the greatest variation in intensity among the various titanium oxides examined. The e_g orbitals point directly to the ligands and as a result the projection of their energy levels in X-ray absorption spectra provides a signature of the cation site environment. It is evident from the comparison of *L*-edge spectra provided in Figure 4b that the line shape of the L_3-e_g band is sensitive to the symmetry of the cation. For all samples the e_g band is split into an asymmetric doublet, the origins of which have been explained through a number of interpretations. Kucheyev *et al.*[51] discussed these recently in their study of titanium oxide aerogels, and through comparisons with amorphous titanium oxide suggested long-range order effects contribute to the line shapes. Based on a negligible change in peak positions with reduction in sample temperature, they also suggested that the dynamic Jahn-Teller effect is not a major contributor to the e_g band splitting. Calculations of the expected Ti $L_{2,3}$ absorption-edge shapes performed by Crocombette *et al.*[52] determined that the influence of first-neighbor interactions cannot account for the large e_g splitting observed in these spectra. This was recently explicitly confirmed in a study by Krüger[49], which reported Ti $L_{2,3}$-edge absorption spectra as simulated by the first-principles multichannel multiple-scattering method, with large numbers of TiO_6 clusters. The splitting of the L_3-e_g band could only be reproduced after consideration of a cluster size of about 60 atoms, which corresponds to a length scale of ~1 nm. This analysis of the L_3-e_g band suggests that TiO_2-SnO_2:F differs in its long-range order from the titanium oxide reference crystals. The physical correlate to this electronic structure observation could be the structural discontinuity that occurs at the substrate-film interface. Disorder on this length scale could reflect a strain gradient and/or relaxation in the interfacial TiO_2. The line shape of the L_3-e_g band appears similar to those found for unrelaxed amorphous TiO_2 prepared by ion bombardment of rutile TiO_2.[51] These disorder-induced modifications to the interfacial electronic structure are expected to exist within larger crystals deposited onto SnO_2:F, which would be strained near the interface and relaxed toward bulk properties farther from the interface.

The high-energy region of the Ti 2*p* absorption spectra, located between 468 and 480 eV (Figure 4c), shows variation among anatase, rutile, and the interfacial TiO_2. This energy range contains two bands separated by 5-6 eV, which have been suggested to originate from $2p_{3/2}$ and $2p_{1/2}$ transitions,[51] as discussed above. The line shapes of these features have been attributed to polaronic transitions,[53] the partial Ti 3*d* and Ti 4*s* density-of-states,[50] and in the molecular orbital description to transitions from Ti 2*p* core levels to t_{1u}-type orbitals.[51,54] The peaks' doublet structure, most evident in the spectrum for anatase TiO_2, is not resolved in the spectrum for TiO_2-SnO_2:F. Generally we observe broadening of the peaks, which is consistent with the disruption of long-range order discussed above with respect to the L_3-e_g band.

Observation of unique ordering on a length scale of 1 nm in interfacial TiO_2 has a number of implications for carrier transport through the TiO_2-SnO_2:F interface during device operation. For example, the corundum crystal structure and associated distorted octahedral symmetry of Ti_2O_3 causes splitting of conduction band t_{2g} states into sub-bands in this material.[55] Specifically, in Ti_2O_3 t_{2g} states are split into bonding and antibonding a_{1g} sub-bands, which surround a e_g^{π} sub-band. This creates a bandgap and results in semiconducting behavior. Although these features of the TiO_2-SnO_2:F interface cannot be determined from data presented in this report, it is interesting to consider the interfacial bonding environment is associated with a number of possible conduction band structures. The unique dispersion of the interfacial Ti 3*d* band, projected onto O *p* orbitals in O l*s* absorption spectra in Figure 3, provides additional evidence of the type of long-range order to which these data refer.

TiO_2-SnO_2:F interfaces in solar cells

The data presented in this report suggest the electronic structure of the TiO_2-FTO interface contrasts with that of its constituent reference crystals through distinct alterations of the crystal-field and long-range order of the cation site environment. These observations provide evidence toward understanding the operation of optoelectronic devices utilizing this interface, which often possess feature dimensionality on the length scale over which the interface was probed in this study. For example, dye-sensitized solar cells commonly utilize as electron transport phases colloidal films of TiO_2 nanoparticles whose diameter is on the order of ten nanometers.[12] The nature of the TiO_2-SnO_2:F interface may play a critical role in determining the performance of these devices. It is generally interpreted that the open circuit potential of dye-sensitized solar cells is limited by the energy difference between the TiO_2 conduction band and the redox potential of the electrolyte.[56] However, the TiO_2-SnO_2:F interface can significantly influence operating parameters such as the fill factor.[57] Rühle and Cahen[57] analyzed the electrostatic potential distribution at the TiO_2-SnO_2:F interface and simulated cell performance with an analytical expression for electron tunneling through an electrostatic barrier. The potential distribution from this analysis suggests the existence of a TiO_2-SnO_2:F interfacial potential barrier width of approximately 1 nm. This is the same length scale over which we observe distinct dissimilarities between the electronic structure of the interface and those of reference titania crystals. Inorganic solid-state solar cells with similar anode architectures, such as extremely-thin-absorber cells,[20] require compact TiO_2 thin films to prevent recombination current during operation. In such cells the potential distribution in this layer should be engineered to promote the efficient injection of electrons from TiO_2 into SnO_2:F. For example, photocurrent transient measurements performed by Rühle and Dittrich[58] suggest increased narrowness of the electrostatic potential drop at the TiO_2-SnO_2:F interface may be required to increase the performance of such cells. In most applications, the translation of electrochemical potential of electrons in TiO_2 to an electrostatic potential at the TiO_2-SnO_2;F interface[56] is expected to be influenced by the unoccupied density-of-states studied experimentally in this report. The description of the electronic structure provided by these measurements suggests, for example, that in non-equilibrium conditions (*i.e.* solar cell operating conditions), the quasi-Fermi level of electrons in the interface will differ from what is expected by consideration of the respective bulk semiconductor properties of the constituent phases. These observations can also relate to the creation of favorable gradients of electrical or chemical potential, which could contribute to the observed high efficiency of dye-sensitized solar cells.

IV. Conclusion

The electronic structure of the TiO_2-FTO interface, an important structure for a number of (opto)electronic devices, has been investigated by soft X-ray absorption spectroscopy. The distinct interfacial electronic structure of TiO_2-FTO has been established by contrasting spectra with those for anatase and rutile TiO_2, FTO, and the ZnO-FTO and CdO-FTO interfaces. The Ti 3*d* band of the interfacial oxygen 1*s* absorption spectrum indicates a reduction in the degree of *p*-*d* hybridization and an alteration of the TiO_2 crystal field. Titanium 2*p* absorption spectra provide evidence for distortion of long-range order around Ti ions in the interfacial TiO_2.

These observations can inform methodology to address operational deficiencies associated with the TiO_2-FTO interface in optoelectronic devices. For example, a comprehensive characterization of the chemically-resolved interfacial electronic structure provides information that facilitates the elimination of unfavorable processing conditions, for example high temperatures, which are associated with additional costs and diffusion effects between phases, and which preclude the use of inexpensive temperature-sensitive substrates. The results indicate that in solar cell operating conditions, the quasi-Fermi level of electrons in the interface will differ from predictions based on bulk oxide material properties. The interfacial electronic structure in addition influences the electrostatic potential distribution at the oxide-TCO interface, which is often a critical operational aspect of working optoelectronic devices. The description of the unoccupied electronic states at the TiO_2-SnO_2:F interface presented in this report provides additional information toward explaining deviations in solar cell performance metrics from those expected by bulk material properties and the various predictive models.

Acknowledgements

This research has been supported by the U.S. Department of Energy, Office of Energy Efficiency and Renewable Energy and Office of Basic Science under Contract No. DE-AC02-05CH11231. M. K. acknowledges support from both the Swedish Research Council (VR) and Axel Hultgren´s memorial fund. The ALD was carried out within the Center on Nanostructuring for Efficient Energy Conversion at Stanford University, an Energy Frontier Research Center funded by the U.S. Department of Energy, Office of Science, Office of Basic Energy Sciences under Award No. DE-SC0001060. J. R. B. acknowledges funding from the Department of Defense through the National Defense Science and Engineering Graduate Fellowship and from the National Science Foundation Graduate Fellowship.

References

[1] P. Zubko, S. Gariglio, M. Gabay, P. Ghosez, and J.-M. Triscone, Annu. Rev. Condens. Matter Phys. **2**, 141 (2011).
[2] B. A. Gregg, J. Phys. Chem. B **107**, 4688 (2003).
[3] A. J. Nozik, Nano Lett. **10**, 2735 (2010).
[4] J. Chakhalian, J. W. Freeland, H.-U. Habermeier, G. Cristiani, G. Khaliullin, M. van Veenendaal, and B. Keimer, Science **318**, 1114 (2007).
[5] A. Ohtomo and H. Y. Hwang, Nature **427**, 423 (2004).
[6] A. Brinkman, M. Huijben, M. van Zalk, J. Huijben, U. Zeitler, J. C. Maan, W. G. van der Wiel, G. Rijnders, D. H. A. Blank, and H. Hilgenkamp, Nature Mater. **6**, 493 (2007).
[7] C. X. Kronawitter, J. R. Bakke, D. A. Wheeler, W.-C. Wang, C. Chang, B. R. Antoun, J. Z. Zhang, J.-H. Guo, S. F. Bent, S. S. Mao, and L. Vayssieres, Nano Lett. **11**, 3855 (2011).
[8] L. Vayssieres, J. Phys. Chem. C **113**, 4733 (2009).
[9] L. Vayssieres, C. Persson, and J.-H. Guo, Appl. Phys. Lett. **99**, 183101 (2011).
[10] L. Vayssieres, C. Sathe, S. M. Butorin, D. K. Shuh, J. Nordgren, and J.-H. Guo, Adv. Mater. **17**, 2320 (2005).
[11] P. Ardalan, T. B. Brennan, H. B. R. Lee, J. R. Bakke, I. K. Ding, M. D. McGehee, and S. F. Bent, ACS Nano **5**, 1495 (2011).
[12] M. Grätzel, Inorg. Chem. **44**, 6841 (2005).
[13] N. Tétreault, É. Arsenault, L.-P. Heiniger, N. Soheilnia, J. Brillet, T. Moehl, S. Zakeeruddin, G. A. Ozin, and M. Grätzel, Nano Lett. **11**, 4579 (2011).
[14] M.-H. Kim and Y.-U. Kwon, J. Phys. Chem. C **113**, 17176 (2009).
[15] K. S. Leschkies, R. Divakar, J. Basu, E. Enache-Pommer, J. E. Boercker, C. B. Carter, U. R. Kortshagen, D. J. Norris, and E. S. Aydil, Nano Lett. **7**, 1793 (2007).
[16] A. K. K. Kyaw, X. W. Sun, C. Y. Jiang, G. Q. Lo, D. W. Zhao, and D. L. Kwong, Appl. Phys. Lett. **93**, 221107 (2008).
[17] K. Ernst, A. Belaidi, and R. Könenkamp, Semicond. Sci. Technol. **18**, 475 (2003).
[18] C. Lévy-Clément, R. Tena-Zaera, M. A. Ryan, A. Katty, and G. Hodes, Adv. Mater. **17**, 1512 (2005).
[19] T. Jiang, T. Xie, Y. Zhang, L. Chen, L. Peng, H. Li, and D. Wang, Phys. Chem. Chem. Phys. **12**, 15476 (2010).
[20] R. Könenkamp, R. C. Word, and C. Schlegel, Appl. Phys. Lett. **85**, 6004 (2004).
[21] *On Solar Hydrogen & Nanotechnology*; L. Vayssieres ed., John Wiley and Sons: Singapore, 2009.
[22] L. Vayssieres, Adv. Mater. **15**, 464 (2003).
[23] T. Ma, M. Guo, M. Zhang, Y. Zhang, and X. Wang, Nanotechnology **18**, 035605 (2007).
[24] K. Zhu, E. A. Schiff, N.-G. Park, J. van de Lagemaat, and A. J. Frank, Appl. Phys. Lett. **80**, 685 (2002).
[25] Y. Ling, G. Wang, D. A. Wheeler, J. Z. Zhang, and Y. Li, Nano Lett. **11**, 2119 (2011).
[26] S. Gutmann, M. A. Wolak, M. Conrad, M. M. Beerbom, and R. Schlaf, J. Appl. Phys. **109**, 113719 (2011).
[27] J. T. Tanskanena, J. R. Bakke, T. A. Pakkanen, and S. F. Bent, J. Vac. Sci. Technol. A **29**, 031507 (2011).
[28] V. E. Henrich, Rep. Prog. Phys. **48**, 1481 (1985).
[29] G. Korotcenkov, Mater. Sci. Eng. B **139**, 1 (2007).
[30] J.-H. Guo, L. Vayssieres, C. Persson, R. Ahuja, B. Johansson, and J. Nordgren, J. Phys.: Condens. Matter **14**, 6969 (2002).
[31] J. Lahiri, S. Senanayake, and M. Batzill, Phys. Rev. B **78**, 155414 (2008)
[32] L. F. J. Piper, L. Colakerol, P. D. C. King, A. Schleife, J. Zúñiga-Pérez, P.-A. Glans, T. Learmonth, A. Federov, T. D. Veal, F. Fuchs, V. Muñoz-Sanjosé, F. Bechstedt, C. F. McConville, and K. E. Smith, Phys. Rev. B **78**, 165127 (2008).
[33] F. M. F. de Groot, M. Grioni, J. C. Fuggle, J. Ghijsen, G. A. Sawatzky, and H. Petersen, Phys. Rev. B **40**, 5715 (1989).
[34] M. Abbate, F. M. F. de Groot, J. C. Fuggle, A. Fujimori, O. Strebel, F. Lopez, M. Domke, G. Kaindl, G. A. Sawatzky, M. Takano, Y. Takeda, H. Eisaki, and S. Uchida, Phys. Rev. B **46**, 4511 (1992).
[35] C. McGuinness, C. B. Stagarescu, P. J. Ryan, J. E. Downes, D. Fu, K. E. Smith, and R. G. Egdell, Phys. Rev. B **68**, 165104 (2003).
[36] J. Chouvin, J. Olivier-Fourcade, J. C. Jumas, B. Simon, Ph. Biensan, F. J. Fernández Madrigal, J. L. Tirado, and C. Pérez Vicente, J. Electroanal. Chem. **494**, 136 (2000).
[37] H. Thakur, R. Kumar, P. Thakur, N. B. Brookesc, K. K. Sharma, A. P. Singh, Y. Kumar, S. Gautam, and K. H. Chae, Chem. Phys. Lett. **511**, 322 (2011).
[38] K. C. Mishra, K. H. Johnson, and P. C. Schmidt, Phys. Rev. B **51**, 13972 (1995).
[39] S. O. Kucheyev, T. F. Baumann, P. A. Sterne, Y. M. Wang, T. van Buuren, A. V. Hamza, L. J. Terminello, and T. M. Willey, Phys. Rev. B **72**, 035404 (2005).
[40] H.-J. Ahn, H.-C. Choi, K.-W. Park, S.-B. Kim, and Y.-E. Sung, J. Phys. Chem. B **108**, 9815 (2004).
[41] X. T. Zhou, J. G. Zhou, M. W. Murphy, J. Y. P. Ko, F. Heigl, T. Regier, R. I. R. Blyth, and T. K. Sham, J. Chem. Phys. **128**, 144703 (2008).
[42] X. T. Zhou, F. Heigl, M. W. Murphy, T. K. Sham, T. Regier, I. Coulthard, and R. I. R. Blyth, Appl. Phys. Lett. **89**, 213109 (2006).
[43] L. Soriano, M. Abbate, J. Vogel, J. C. Fuggle, A. Fernández, A. R. González-Elipe, M. Sacchi, and J. M. Sanz, Surf. Sci. **290**, 427 (1993).
[44] D. W. Fischer and W. L. Baun, J. Appl. Phys. **39**, 4757 (1968).
[45] F. M. F. de Groot, M. O. Figueiredo, M. J. Basto, M. Abbate, H. Petersen, and J. C. Fuggle, Phys. Chem. Miner. **19**, 140 (1992).
[46] A. G. Thomas, W. R. Flavell, A. K. Mallick, A. R. Kumarasinghe, D. Tsoutsou, N. Khan, C. Chatwin, S. Rayner, G. C. Smith, R. L. Stockbauer, S. Warren, T. K. Johal, S. Patel, D. Holland, A. Taleb, and F. Wiame, Phys. Rev. B **75**, 035105 (2007).
[47] X. Chen, P.-A. Glans, X. Qiu, S. Dayal, W. D. Jennings, K. E. Smith, C. Burda, and J.-H. Guo, J. Electron Spectrosc. Relat. Phenom. **162**, 67 (2008).
[48] H. Ikeno, F. M. F de Groot, E. Stavitski, and I. Tanaka, J. Phys.: Condens. Matter **21**, 104208 (2009).
[49] P. Krüger, Phys. Rev. B **81**, 125121 (2010).
[50] L. D. Finkelstein, E. I. Zabolotzky, M. A. Korotin, S. N. Shamin, S. M. Butorin, E. Z. Kurmaev, and J. Nordgren, X-ray Spectrom. **31**, 414 (2002).
[51] S. O. Kucheyev, T. van Buuren, T. F. Baumann, J. H. Satcher, Jr., T. M. Willey, R. W. Meulenberg, T. E. Felter, J. F. Poco, S. A. Gammon, and L. J. Terminello, Phys. Rev. B **69**, 245102 (2004).

[52] J. P. Crocombette and F. Jollet, J. Phys.: Condens. Matter **6**, 10811 (1994).
[53] G. van der Laan, Phys. Rev. B **41**, 12366 (1990).
[54] J. A. Tossell, D. J. Vaughan, and K. H. Johnson, Am. Mineral. **59**, 319 (1974).
[55] A. T. Paxton and L. Thiên-Nga, Phys. Rev. B **57**, 1579 (1998).
[56] J. Bisquert, D. Cahen, G. Hodes, S. Rühle, and A. Zaban, J. Phys. Chem. B **108**, 8106 (2004).
[57] S. Rühle and D. Cahen, J. Phys. Chem. B **108**, 17946 (2004).
[58] S. Rühle and T. Dittrich, J. Phys. Chem. B **109**, 9522 (2005).